# Thermohaline Circulation Enhanced by Wind Forcing

HIROYUKI TSUJINO AND NOBUO SUGINOHARA

*Center for Climate System Research, University of Tokyo, Tokyo, Japan*

(Manuscript received 3 February 1998, in final form 27 July 1998)

ABSTRACT

A thermohaline circulation enhanced by wind forcing is demonstrated in an idealized basin model, and a mechanism that provides a connection between wind forcing and a thermohaline circulation is clarified. A rectangular ocean that extends over the Northern and Southern Hemispheres is driven by differential heating and wind stress at the sea surface. The differential heating is so distributed that the deep water is formed at the southern end of the model ocean. The wind stress is so distributed that there are three wind-driven gyres in the Northern Hemisphere, and it is not imposed in the Southern Hemisphere. Comparison is made between the cases with and without the wind stress. When the wind forcing is imposed, the basin-scale meridional circulation increases in intensity. This is due to the enhanced surface heating in the cyclonic wind-driven gyre with the Ekman upwelling and the accompanying enhanced surface cooling in the deep-water formation region. In the cyclonic wind-driven gyre, the Ekman upwelling brings up the thermocline to the subsurface depths to enhance the surface heating and also the downward heat conduction from the sea surface to the deep layer, which leads to warming of the deep water. Thus, the enhanced surface heating in the cyclonic gyre is balanced with the enhanced surface cooling in the deep-water formation region due to the warmed deep water. In this way, the wind forcing enhances a thermohaline circulation that connects the deep-water formation region to the cyclonic wind-driven gyre with the Ekman upwelling.

## 1. Introduction

The thermohaline circulation is driven by the thermohaline forcing due to distribution of the heat and the freshwater flux through the sea surface. It is considered to take the form that the high density water formed in the concentrated region by convection upwells in the rest of the ocean to balance with downward conduction from the sea surface.

The wind forcing due to distribution of the wind stress over the ocean causes the Ekman upwelling/downwelling, and then it drives the wind-driven circulation. Since the Ekman *downwelling* pushes down the surface water and causes the circulation associated with the ventilated thermocline (Luyten et al. 1983), the thermohaline circulation is insulated from the thermohaline forcing in the subtropical gyre, as argued by Samelson and Vallis (1997). On the other hand, the Ekman *upwelling* brings up the deep water to the subsurface depths and exposes it to the thermohaline forcing, which may cause a large heat gain in the region with the Ekman upwelling. Thus, the Ekman upwelling may force the conversion of dense deep water masses to the surface waters with much lower density. This implies an enhancement of the replacement rate of the deep water and an amplification of the thermohaline circulation.

In fact, Toggweiler and Samuels (1995) pointed out that the formation of the North Atlantic Deep Water (NADW) and the outflow of NADW from the Atlantic are closely related to the wind stress over the Southern Ocean. They suggested the importance of the Ekman upwelling over the Southern Ocean in bringing up NADW to the sea surface.

In the North Pacific modeling of Tsujino and Suginohara (1998), a large difference in meridional circulation at the subthermocline depths between cases with and without wind stress is found. That is, the upper circulation cell in the layered deep Pacific meridional circulation (Obata et al. 1996) is greatly intensified when the wind forcing is imposed. The strong circulation at the subthermocline depths is also found in the Pacific model of Ishizaki (1994) and in the World Ocean circulation model of Nakata and Suginohara (1998). There seems to exist a large northward transport at middepths and a large southward transport near the sea surface for the meridional circulation in the Pacific, being caused by the wind forcing.

The purpose of the present study is to demonstrate a thermohaline circulation enhanced by the wind forcing in an idealized basin model and to clarify a mechanism that provides a connection between the wind forcing and the thermohaline circulation. We carry out numer-

*Corresponding author address:* Dr. Hiroyuki Tsujino, Center for Climate System Research, University of Tokyo, 4-6-1 Komaba, Meguro-ku, Tokyo 153-8904, Japan.

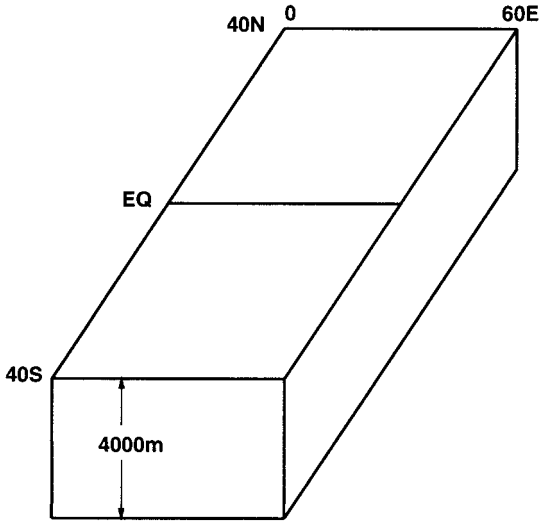


FIG. 1. Schematic view of the model ocean.

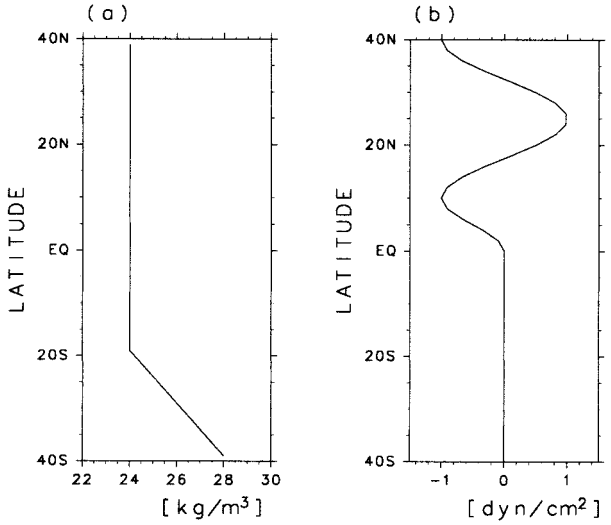


FIG. 2. Meridional distribution of (a) the reference density and (b) the wind stress.

ical experiments for a single closed basin model with the deep-water formation in the Southern Hemisphere and the wind forcing in the Northern Hemisphere. Three case studies are made by changing the wind stress distribution to understand how the wind forcing affects the thermohaline circulation. First, the ocean is driven only by the thermohaline forcing. Next, the wind forcing is imposed and modification of the circulation is examined. The circulation driven by the wind stress with reversed direction is also calculated to understand if results depend on a particular wind stress distribution. Sensitivity to the vertical diffusivity and the meridional distribution of the thermohaline forcing is also investigated. Then, we will identify a mechanism that provides a connection between the wind forcing and the thermohaline circulation. To accomplish this, we carry out some supplementary experiments in which a result for the case with wind stress is reproduced in a case without wind stress by parameterizing effects of the wind forcing.

This paper is organized as follows. Section 2 describes the model. Results of calculations are presented in section 3, and the mechanism is discussed in section 4. Section 5 presents a summary and discussion.

## 2. Experimental design

A rectangular ocean that extends over the Northern and Southern Hemispheres as shown in Fig. 1 is considered. The latitudinal width is 80° and the longitudinal width is 60°. The ocean has a flat bottom and is 4000 m deep.

The forcing agents are the buoyancy forcing and the wind forcing at the sea surface. The buoyancy forcing is made by restoring density to the reference value with the damping time of 60 days. The reference density, $\rho_*$, for the surface buoyancy forcing and the imposed zonal component of the wind stress are shown in Figs. 2a and 2b. They are zonally uniform. The reference density is so distributed that the deep water is formed at the southern end of the model ocean. The wind stress is so distributed that there are three wind-driven gyres in the Northern Hemisphere, and it is not imposed in the Southern Hemisphere.

Three cases with different wind stress distribution are carried out. First, the ocean is forced only by the sea surface reference density distribution in Fig. 2a (case I). Next, two types of wind stress distribution are imposed for case I. In one case the wind stress is that shown in Fig. 2b (case II). In the other case the direction of the wind in Fig. 2b is reversed (case III). For cases I and II, sensitivity to the vertical diffusivity is examined by taking the larger vertical diffusivity (cases $I_{DIF}$ and $II_{DIF}$). Also sensitivity to the meridional distribution of the buoyancy forcing is examined by introducing the meridional gradient to the reference density (cases $I_{DRD}$ and $II_{DRD}$).

Reproduction experiments are also carried out. Case $I_{LED}$ is one of the cases where the vertical diffusivity is locally enhanced for case I. The cases are listed in Table 1.

We use the Center for Climate System Research Ocean General Circulation Model (CCSR-OGCM). The CCSR-OGCM is a multilevel model that solves the primitive equations under the hydrostatic, Boussinesq, and rigid-lid approximation. The finite differencing method is the same as that of Suginohara and Aoki (1991), where the weighted upcurrent scheme is adopted for the advection terms of density. Unstable stratification is removed by convective adjustment: when potential density at a certain grid point is larger than that just below, the potential density is homogenized downward

TABLE 1. List of experiments.

| Case | Wind | Vertical diffusivity | Reference density in N. Hemisphere |
|---|---|---|---|
| I | Off | 0.3 $cm^2\ s^{-1}$ | Constant (Fig. 2a) |
| II | On | 0.3 $cm^2\ s^{-1}$ | Constant (Fig. 2a) |
| III | Reversed | 0.3 $cm^2\ s^{-1}$ | Constant (Fig. 2a) |
| $I_{DIF}$ | Off | 1.0 $cm^2\ s^{-1}$ | Constant (Fig. 2a) |
| $II_{DIF}$ | On | 1.0 $cm^2\ s^{-1}$ | Constant (Fig. 2a) |
| $I_{DRD}$ | Off | 0.3 $cm^2\ s^{-1}$ | Distributed (Fig. 10) |
| $II_{DRD}$ | On | 0.3 $cm^2\ s^{-1}$ | Distributed (Fig. 10) |
| $I_{LED}$ | Off | Locally enhanced* | Constant (Fig. 2a) |

* See text.

from that grid point until unstable stratification is completely removed.

The horizontal resolution is $2° \times 2°$, and there are 32 levels in the vertical with high resolution near the sea surface (50 m) and decreased resolution toward the bottom (200 m).

We use the following values for the model parameters: $A_H = 8.0 \times 10^8\ cm^2\ s^{-1}$, $A_V = 1.0\ cm^2\ s^{-1}$, $K_H = 1.0 \times 10^7\ cm^2\ s^{-1}$, and $K_V = 0.3\ cm^2\ s^{-1}$, where $A_H$ and $A_V$ are the horizontal and the vertical viscosity coefficient, and $K_H$ and $K_V$ are the horizontal and the vertical diffusion coefficient.

The model equations are integrated for more than 6000 years to obtain a thermally and dynamically steady state, using Bryan's acceleration method (Bryan 1984).

## 3. Results

The zonally integrated meridional transport streamfunction for cases I through III is shown in Fig. 3. In case I without the wind stress, a typical meridional circulation forms due to the buoyancy-driven circulation (e.g., Suginohara and Aoki 1991). The deep water is formed at the southern end of the model ocean and the water slowly upwells in the rest of the ocean, which establishes the large meridional circulation cell. When the wind forcing is imposed, the Ekman cells are formed in the upper layer and the large meridional circulation cell is significantly intensified. In the region where the wind forcing induces Ekman upwelling, that is, in the cyclonic wind-driven gyre, the deep upwelling seems to be connected to the Ekman upwelling as seen for cases II and III. Comparison between cases II and III shows that the intensity of the large meridional circulation cell is almost the same in the two cases, though the circulation pattern in the Northern Hemisphere is slightly different. This indicates that the buoyancy-driven (thermohaline) circulation increases in intensity irrespective of the direction of the wind stress.

Zonally averaged density for cases I through III is shown in Fig. 4. The dense water formed at the southern end of the model ocean occupies the depths below the pycnocline. Density is almost meridionally uniform north of the deep-water formation region in case I. In

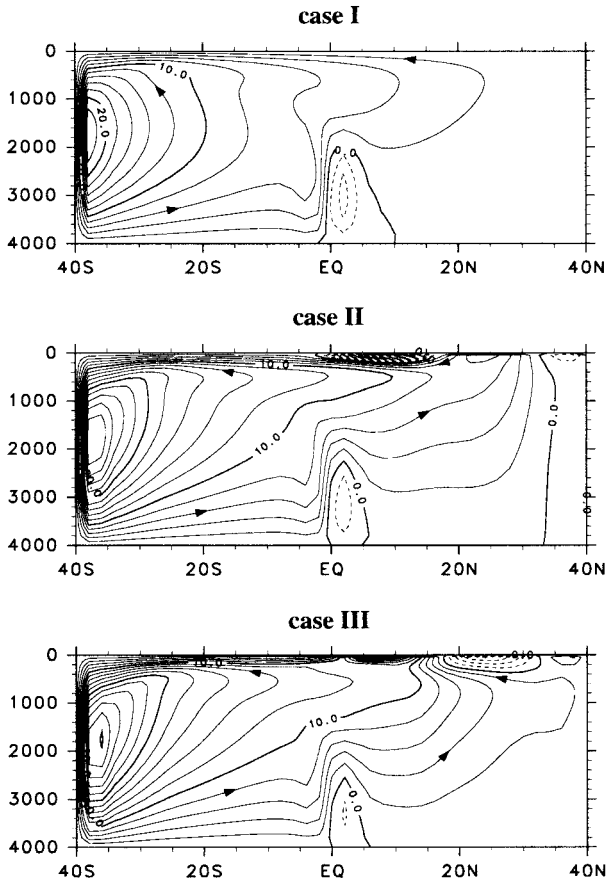


FIG. 3. Zonally integrated mass transport streamfunction for cases I–III in Sv (Sv $\equiv 10^6\ m^3\ s^{-1}$) units. Contour interval is 2 Sv.

cases II and III, isopycnals are sucked up in the cyclonic wind-driven gyre with the Ekman upwelling and are pushed down in the anticyclonic gyre with Ekman downwelling. Density in the deep layer decreases when the wind forcing is imposed (see also Fig. 8).

Zonally averaged zonal velocity for cases I through III is shown in Fig. 5. In the Northern Hemisphere, strong flows associated with the wind-driven circulation are found in cases II and III, and they are confined to the upper 1000-m depths. The three cases show a similar flow pattern in the deep layer except in the northern part of the Northern Hemisphere where the wind-driven circulation dominates, that is, the wind-driven circulation penetrates into the deep layer. It is clearly seen that the flow in the Southern Hemisphere strengthens when the wind stress is imposed though the structure is almost the same as that of case I. Thus, the intensity of the buoyancy-driven circulation is greatly affected by the wind forcing.

Figures 6a and 6b show the pressure field for cases I through III at depths of 75 m and 3100 m, respectively.

At 75 m (Fig. 6a), in case I, the anticyclonic gyre in the Northern Hemisphere is connected to the strong southward western boundary current in the Southern

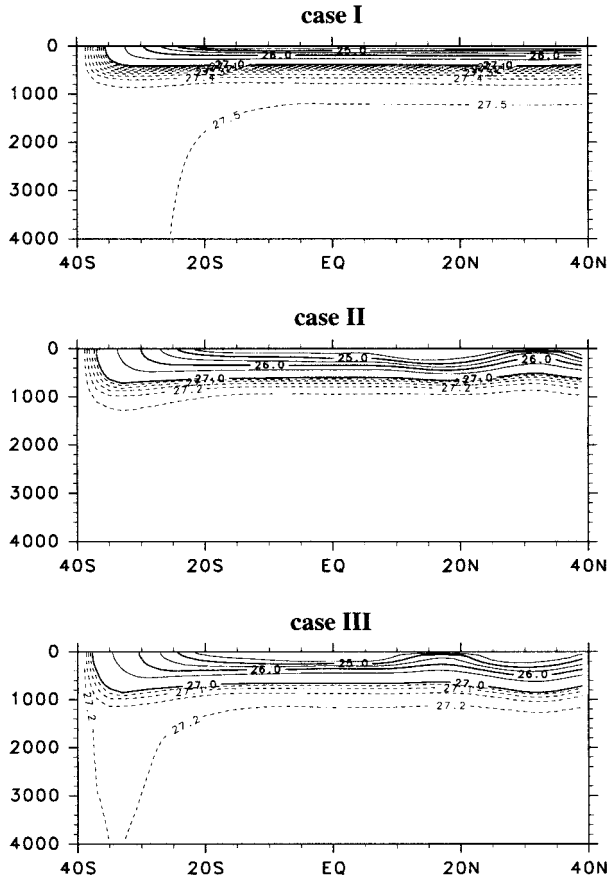


FIG. 4. Zonally averaged potential density ($\sigma_\theta$) for cases I–III. Contour interval is 0.5 $\sigma_\theta$. For density greater than 27.0 $\sigma_\theta$, contour interval is 0.05 $\sigma_\theta$.

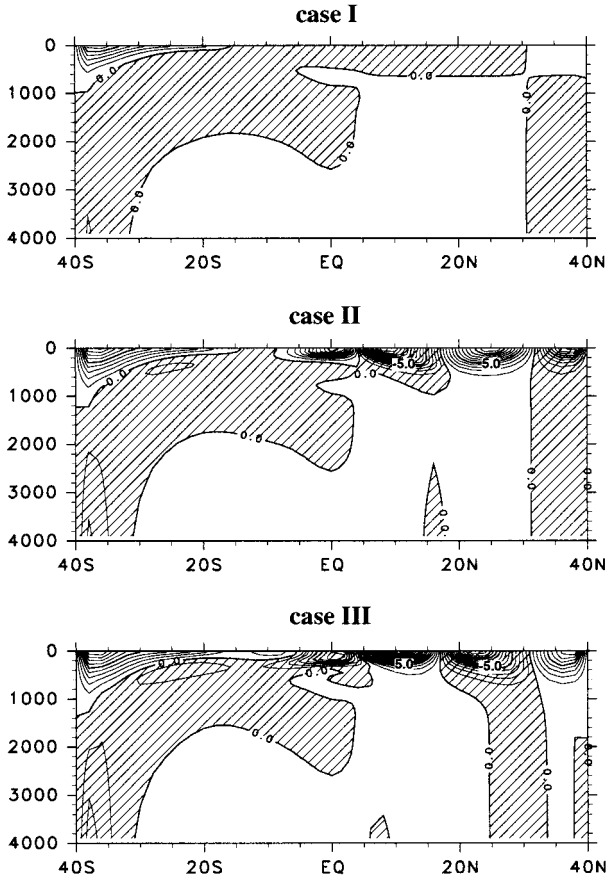


FIG. 5. Zonally averaged zonal velocity for cases I–III. Contour interval is 1.0 cm $s^{-1}$. The shaded regions indicate the westward flow.

Hemisphere, which is the upper-layer circulation pattern associated with the Stommel–Arons deep circulation for the Pacific (Suginohara and Aoki 1991). When the wind forcing is imposed, three wind-driven gyres are formed in the Northern Hemisphere though the flow direction of the gyres is opposite between cases II and III. The southward western boundary current as well as the interior eastward flow in the Southern Hemisphere is stronger for cases II and III.

At 3100 m (Fig. 6b), in case I, the Stommel–Arons deep circulation pattern for the Pacific is formed; that is, the northward deep western boundary current originating from the deep-water formation region crosses the equator and feeds the cyclonic circulation in the Northern Hemisphere. When the wind forcing is imposed, the circulation in the Southern Hemisphere becomes stronger for both cases II and III. In the Northern Hemisphere, for case II the cyclonic circulation becomes much stronger, and for case III the cyclonic circulation becomes stronger, but its center shifts to about 20°N. It is noted that, as seen in Fig. 5, the wind-driven circulation tends to penetrate into the deep layer in the northern part of the Northern Hemisphere.

Effects of the wind forcing on the buoyancy-driven circulation will be more clearly seen in the difference between the cases with and without the wind stress. The difference of the meridional transport streamfunction between the cases (case II − case I) and (case III − case I) is shown in Fig. 7. The basin-scale meridional circulation increases in intensity at all depths. The concentrated upwelling from the deep layer occurs in the region where the Ekman upwelling is taking place, and the upwelled deep water comes directly from the deep-water formation region in the Southern Hemisphere without notable upwelling along the way. This suggests that the strength of the intensified circulation does not strongly depend upon the vertical diffusivity, a crucial parameter for controlling the intensity of the thermohaline circulation. The effect of wind forcing on the meridional circulation is not confined to the upper layer. The wind forcing affects the intensity and structure of the large-scale buoyancy-driven (thermohaline) circulation.

The difference of the zonally averaged density between the cases (case II − case I) and (case III − case I) is shown in Fig. 8. When the wind forcing is imposed,

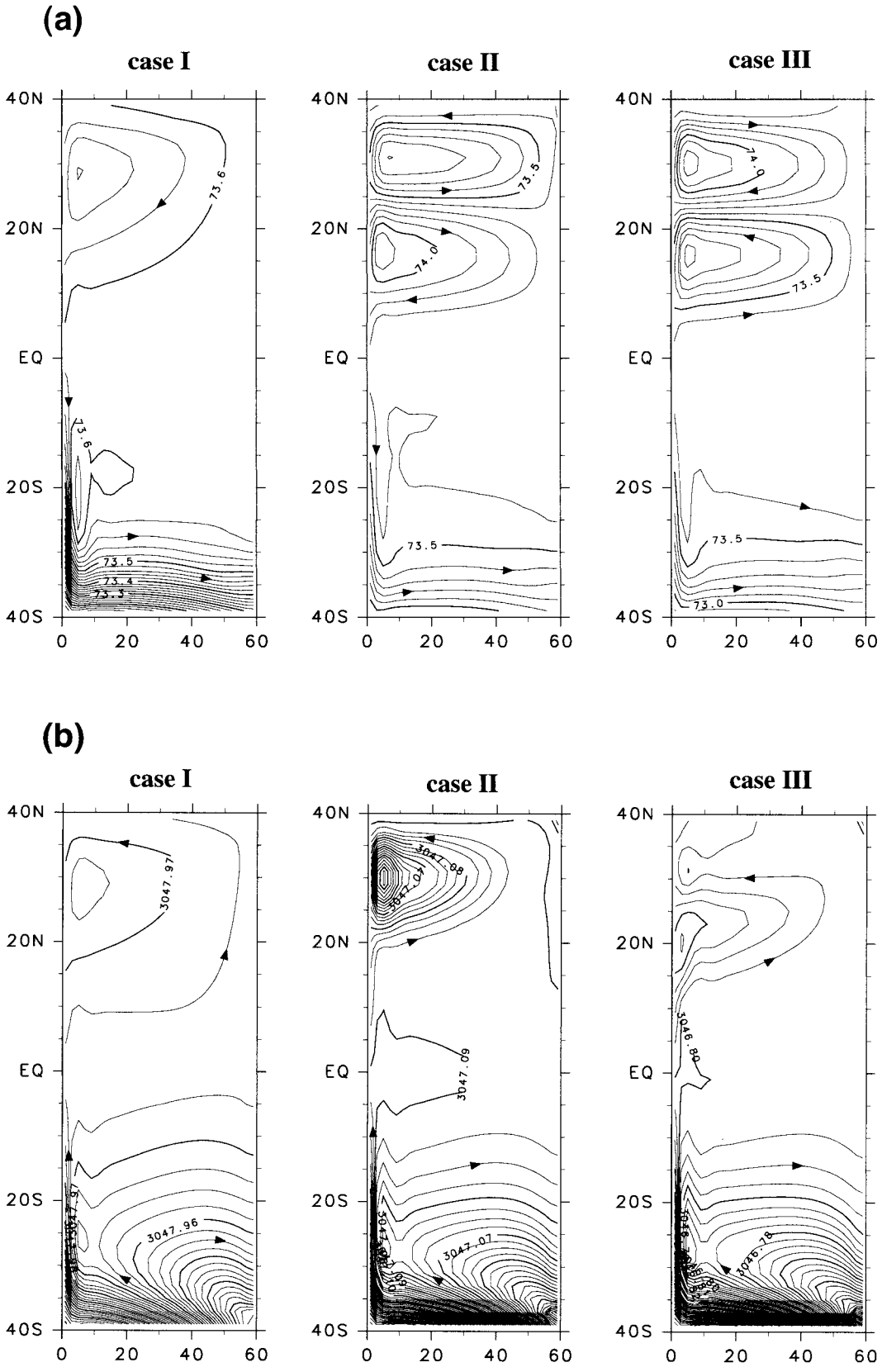


FIG. 6. Pressure at the depths of (a) 75 m and (b) 3100 m for cases I–III (in db). (a) Contour interval is 0.02 db for case I and 0.1 db for cases II and III. (b) Contour interval is 0.0025 db.

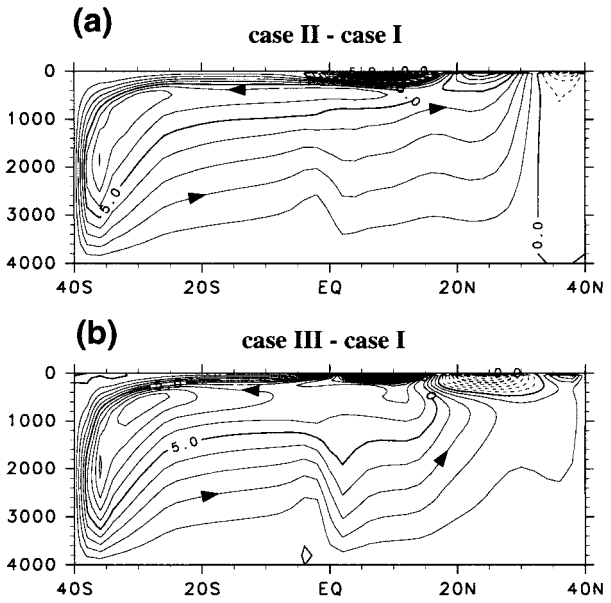


FIG. 7. Difference of zonally integrated mass transport streamfunction: (a) (case II − case I) and (b) (case III − case I) in Sv units. Contour interval is 1 Sv.

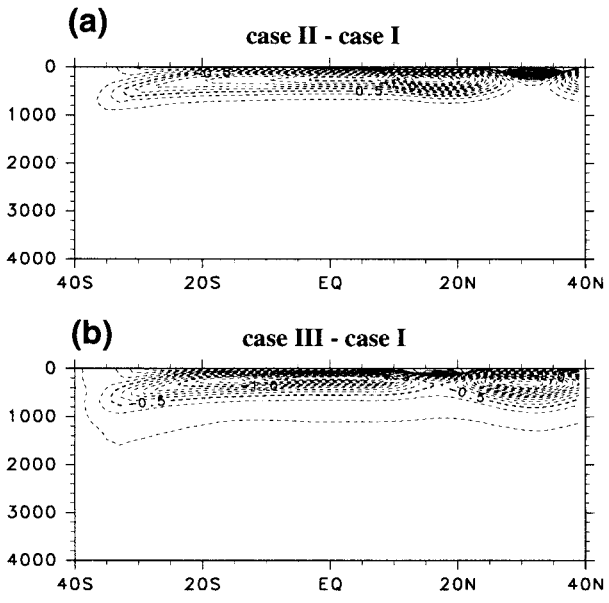


FIG. 8. Difference of zonally averaged density: (a) (case II − case I) and (b) (case III − case I) in $\sigma_\theta$. Contour interval is 0.1 $\sigma_\theta$.

density becomes lower in most of the ocean (most of the ocean is warmed) except near the sea surface in the region with the Ekman upwelling. There, isopycnals are sucked up and hence the density becomes higher compared with the case without wind stress. Thus, the buoyancy (heat) budget through the sea surface may be greatly modified.

Sensitivity to the vertical diffusivity is examined. Differences between cases $I_{DIF}$ and $II_{DIF}$ where the vertical diffusion coefficient is taken to be larger, $K_V = 1.0$ cm$^2$ s$^{-1}$, are shown in Fig. 9. The circulation in each case becomes stronger due to the larger diffusivity (not shown here). But, the differences of both the meridional transport streamfunction and the zonally averaged density are slightly smaller while their structures are not different than those in the small diffusivity case (cf. Figs. 7a and 8a). The meridional circulation is less intensified with increasing vertical diffusivity.

Sensitivity to the meridional distribution of the buoyancy forcing is also examined by introducing the meridional gradient to the reference density (cases $I_{DRD}$ and $II_{DRD}$). The reference density, the meridional transport streamfunction for cases $I_{DRD}$ and $II_{DRD}$, and the difference (case $II_{DRD}$ − case $I_{DRD}$) are shown in Fig. 10. The zonally averaged density for these cases and the difference are shown in Fig. 11. The maximum value of the reference density at the northern end is set to be lower than that at the southern end (Fig. 10). It is clearly seen also in this case that the wind forcing leads to the intensification of the basin-scale meridional overturning circulation and the warming of the deep water (cf. Figs. 7a and 8a). A remarkable difference in meridional overturning from cases I and II (Fig. 3) is that a local buoyancy-driven circulation forms at subsurface depths in the Northern Hemisphere. It is noted that, as seen in the difference in Fig. 10, the concentrated deep upwelling is connected to the Ekman upwelling.

A case where the damping time for the restoring boundary condition for density at the sea surface is taken to be 30 days is also calculated in cases I and II. Almost the same results are obtained.

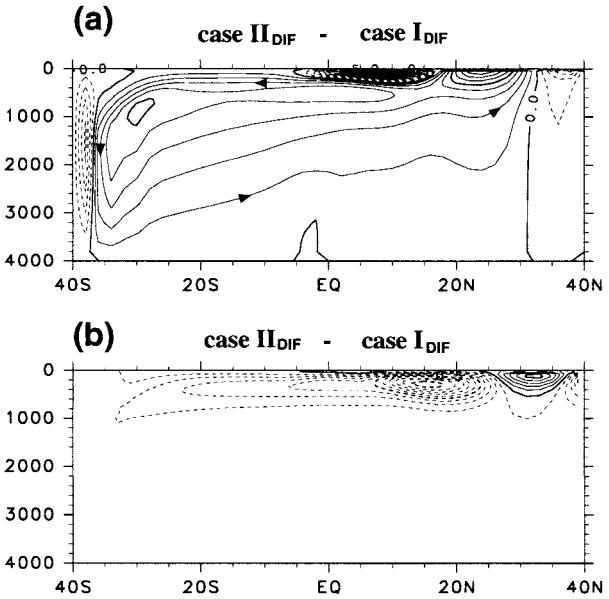


FIG. 9. (a) Difference of zonally integrated mass transport streamfunction in Sverdrups and (b) that of zonally averaged density in $\sigma_\theta$ for (case $II_{DIF}$ − case $I_{DIF}$). Contour intervals are 1 Sv in (a) and 0.1 $\sigma_\theta$ in (b).

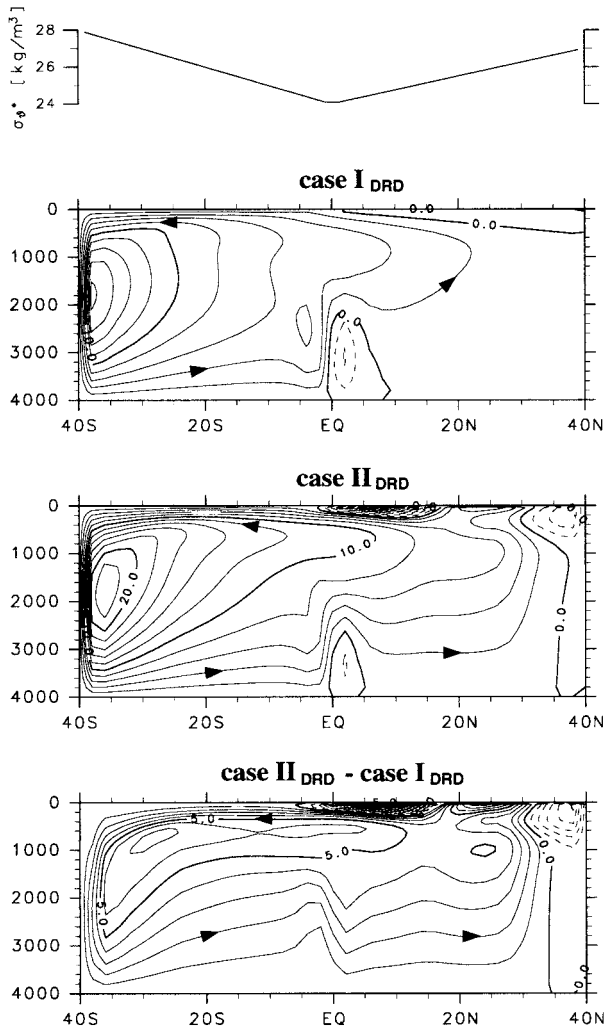


FIG. 10. Reference density, zonally integrated mass transport streamfunction for cases $I_{DRD}$ and $II_{DRD}$ and difference (case $II_{DRD}$ − case $I_{DRD}$) in Sv units. Contour interval for cases $I_{DRD}$ and $II_{DRD}$ is 2 Sv and that for the difference is 1 Sv.

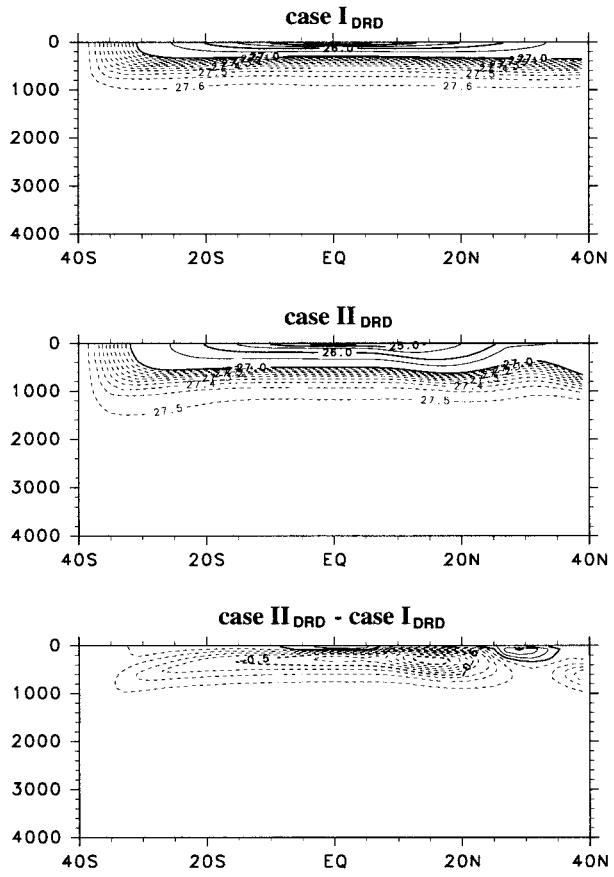


FIG. 11. Zonally averaged potential density ($\sigma_\theta$) for cases $I_{DRD}$ and $II_{DRD}$ and difference (case $II_{DRD}$ − case $I_{DRD}$). Contour interval for cases $I_{DRD}$ and $II_{DRD}$ is 0.5 $\sigma_\theta$. For density greater than 27.0 $\sigma_\theta$, contour interval is 0.05 $\sigma_\theta$. Contour interval for the difference is 0.1 $\sigma_\theta$.

## 4. Mechanism

As shown in section 3, the effect of the wind forcing, even if remote from the deep-water formation region, leads to the intensification of the global meridional overturning circulation, the circulation being less intensified with increasing vertical diffusivity. Then, the problem may be how this circulation is established and whether it can be called a buoyancy-driven (thermohaline) circulation.

The difference between the calculated and the reference density, $\rho - \rho_*$, is depicted in Fig. 12. This value is proportional to the buoyancy (heat) flux through the sea surface. When the wind forcing is imposed, the buoyancy gain (heating) becomes larger in the region with the Ekman upwelling in contrast to the region with the Ekman downwelling. This is because the *upwelled* water in the region with the Ekman upwelling causes a larger difference from the reference value. At the same time, the buoyancy loss (cooling) becomes larger at the southern end of the model ocean. This is due to the lower density (higher temperature) of the deep water (Fig. 8), which causes the larger difference from the reference value in the deep-water formation region. Thus, the buoyancy (heat) budget through the sea surface is greatly modified.

Vertical profiles of the terms in the density equation for the upper 500-m depths in the central subpolar gyre (33°N, 29°E) for cases I and II are shown in Fig. 13 [for the density equation, see Suginohara and Aoki (1991)]. The vertical advection and vertical diffusion terms at the upper 100-m depths become much larger when the wind forcing is imposed. This feature is found everywhere in the subpolar gyre in contrast to the subtropical gyre where the horizontal and vertical advection terms dominate. The deep water brought up to the upper layer in the subpolar gyre with the Ekman upwelling is directly ''heated'' by conduction from the sea surface. Thus, the very active conversion from the deep water of high density to the surface water of low density takes

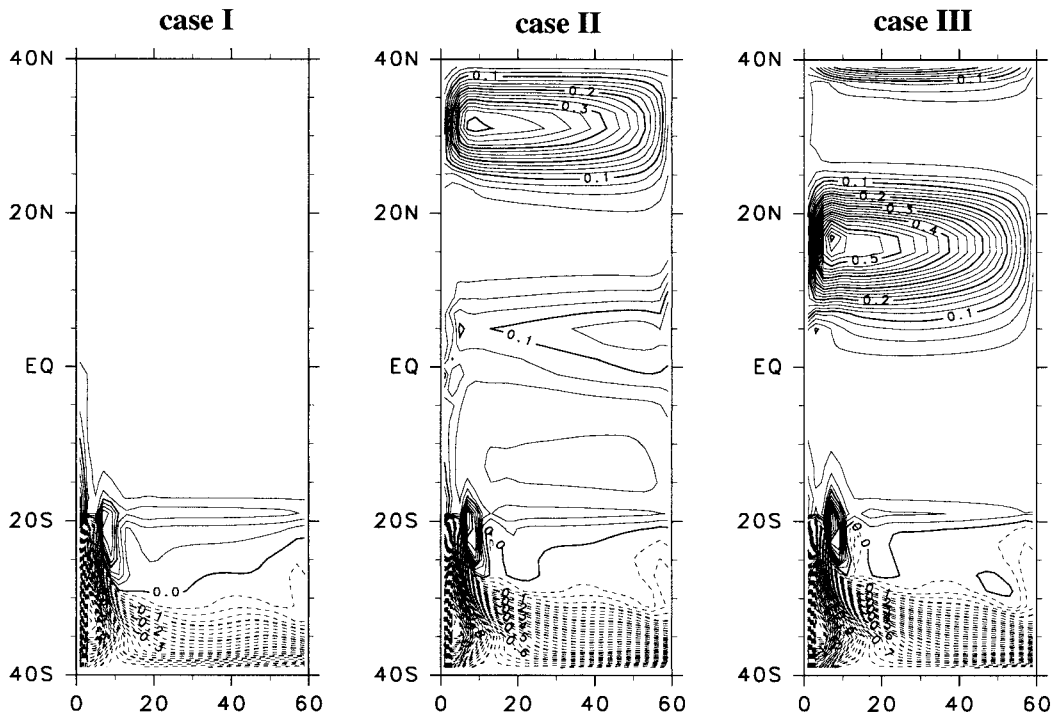


FIG. 12. Difference between the calculated and the reference density at the sea surface ($\rho - \rho_*$) for cases I–III. Contour interval is 0.025 $\sigma_\theta$.

place at the subsurface depths in the subpolar gyre, that is, in the region with the Ekman upwelling.

Therefore, it is understood that in the region with the Ekman upwelling the wind forcing enhances the surface buoyancy flux and changes the density balance at the subsurface depths. It seems that the intensified global meridional overturning circulation seen for the cases with the wind stress is due to a buoyancy-driven (thermohaline) circulation enhanced by the wind forcing. If this is really a buoyancy-driven circulation, the intensified overturning circulation with the enhanced surface buoyancy fluxes should be reproduced for a case without wind stress by reasonably parameterizing the effect of the wind forcing in the density equation. As seen in Fig. 13, the vertical diffusion becomes larger at the pycnocline (thermocline) depths in the subpolar gyre. So, for case I, the vertical diffusion coefficient is significantly increased to $K_V = 3.0$ cm$^2$ s$^{-1}$ in the domain between 30°N and 40°N and between 0 m and 420 m (case $I_{LED}$). The meridional overturn and zonally integrated buoyancy flux for case $I_{LED}$ is shown in Fig. 14. The intensified overturning circulation with the enhanced surface buoyancy fluxes in case II is almost reproduced. In other words, the locally enhanced vertical diffusivity causes a buoyancy-driven circulation that connects the deep-water formation region to the region with enhanced vertical diffusivity. This feature is also reproduced for a case where the vertical advective flux of density due to the effect of wind forcing is imposed on the density equation. Therefore, it is concluded that the intensified overturning circulation is due to a buoyancy-driven (thermohaline) circulation enhanced by the wind forcing. This thermohaline circulation can be called a ''wind-enhanced thermohaline circulation.'' It should be remarked here that the intensified overturning circulation with the enhanced surface buoyancy fluxes is not reproduced even for a case where the surface reference density distribution is greatly modified.

Now, the intensification of the global meridional overturning circulation for the cases with wind stress can be explained as follows: Starting with the steady state of case I, let us impose the wind forcing on it. Isopycnals are sucked up in the cyclonic wind-driven gyre with the Ekman upwelling. There, the ocean gains more buoyancy (is heated) through the sea surface because the upwelled water causes a larger difference in density from the reference value, and also the deep water below the pycnocline gains more buoyancy by the enhanced downward conduction from the sea surface as seen in Fig. 13. As a result, the deep ocean has the lower density (higher temperature) as seen in Figs. 4 and 8. In a steady state, the excess buoyancy gain (heating) must be balanced by the excess buoyancy loss (cooling) somewhere. Considering the efficiency of buoyancy (heat) transfer by convection and conduction, as discussed in Suginohara and Aoki (1991), the compensatory buoyancy loss (cooling) can be done by convection in a very confined region. This occurs only in the deep-water formation region at the southern end of the model ocean as shown in Fig. 12. In fact, the deep

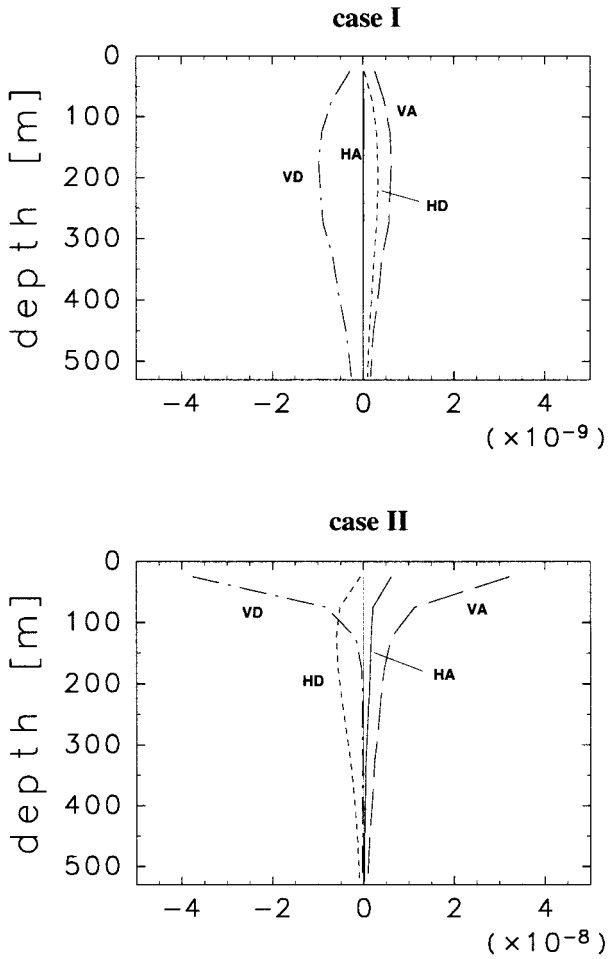


FIG. 13. Vertical profiles of the terms in the density equation for the upper 500-m depths in the central subpolar gyre (33°N, 29°E) for cases I and II. Note that the scale on the abscissa is different between cases I and II. HA: horizontal advection, VA: vertical advection, VD: vertical diffusion, HD: horizontal diffusion. The unit of the abscissa is $\sigma_\theta$ s$^{-1}$.

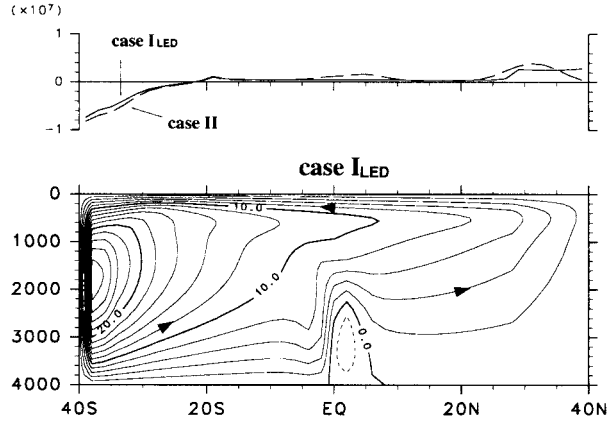


FIG. 14. Meridional overturn in Sv units (lower) and zonally integrated surface buoyancy flux in $\sigma_\theta$ m$^3$ s$^{-1}$ units (upper) for case $I_{LED}$. Contour interval in the lower figure is 2 Sv. The dashed line in the upper figure is for zonally integrated buoyancy flux in case II.

water of lower density (higher temperature) caused by the enhanced downward conduction in the cyclonic gyre leads to the larger difference from the reference density in the deep-water formation region, which leads to a larger buoyancy loss and hence larger production rate of the deep water. Thus, the wind-enhanced thermohaline circulation connecting the deep-water formation region to the cyclonic wind-driven gyre is established.

Next, by using the mechanism understood above, we may explain why the circulation is less intensified with increasing vertical diffusivity (Fig. 9). With the larger vertical diffusivity, the stratification associated with the buoyancy-driven circulation without wind stress becomes diffuse. When the wind forcing is imposed on it, distortion of isopycnals caused by the wind stress penetrates deeper but its amplitude near the sea surface becomes smaller than in the small diffusivity case. The isopycnals coming to the sea surface have lower density due to the diffuse stratification. Thus, the excess buoyancy gain through the sea surface in the cyclonic gyre is not as large as that in the small diffusivity case. Then, the intensity of the wind-enhanced buoyancy-driven (thermohaline) circulation in the large diffusivity case is not as strong as that in the small diffusivity case.

It is interesting to show the buoyancy flux through the sea surface for cases $I_{DRD}$ and $II_{DRD}$ (Fig. 15). As expected from the results in Figs. 10 and 11, the buoyancy gain (heating) in the southern half of the subpolar gyre and the buoyancy loss (cooling) in the deep-water

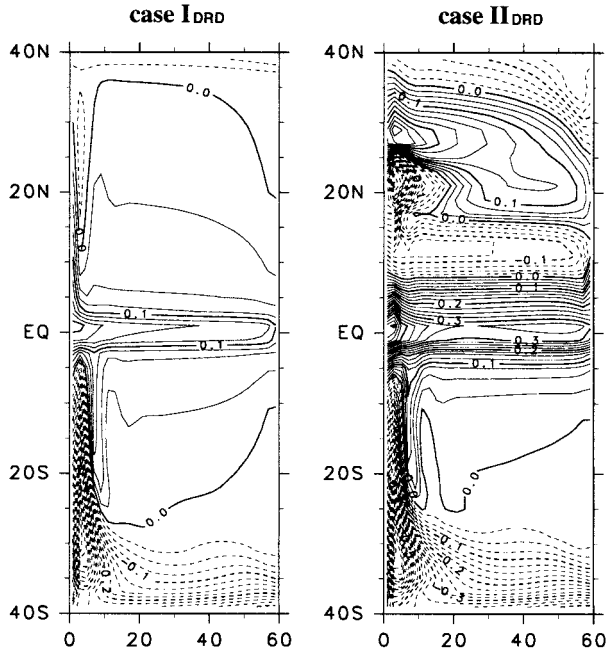


FIG. 15. Difference between the calculated and the reference density at the sea surface ($\rho - \rho_*$) for cases $I_{DRD}$ and $II_{DRD}$. Contour interval is 0.025 $\sigma_\theta$.

formation region become larger when the wind forcing is imposed. The distribution of the buoyancy flux for case $II_{DRD}$ is different than that for case II (Fig. 12). This is due to advection effects of the Ekman transport and the wind-driven western boundary current. This heating and cooling, except the enhanced heating in the southern half of the subpolar gyre, does not significantly affect the basin-scale thermohaline circulation: only the heating in the southern half of the subpolar gyre contributes to the warming of the deep water. Particularly, in the subtropical gyre, the deep water is insulated from the surface heating and cooling, as argued by Samelson and Vallis (1997).

## 5. Summary and discussion

We have investigated the buoyancy-driven (thermohaline) circulation enhanced by wind forcing. A rectangular ocean with a flat bottom is driven by the buoyancy (thermohaline) and the wind forcing at the sea surface. The reference density for the buoyancy forcing is constant except in the southern part of the Southern Hemisphere where the deep water is formed. The wind stress is so distributed that there are three wind-driven gyres in the Northern Hemisphere, and it is not imposed in the Southern Hemisphere. Three cases have been carried out changing wind stress distribution: no wind stress, the wind stress, and the wind stress with opposite direction. When the wind forcing is imposed, the basin-scale meridional circulation increases in intensity. This is due to the enhanced surface buoyancy gain (heating) in the cyclonic wind-driven gyre with Ekman upwelling and the accompanying enhanced surface buoyancy loss (cooling) in the deep-water formation region. In the cyclonic wind-driven gyre, the Ekman upwelling lifts the pycnocline (thermocline) near the sea surface to enhance the surface buoyancy gain (heating) and also the downward conduction from the sea surface to deep layer. This results in deep water of lower density (warming of the deep water), which leads to the enhanced buoyancy loss (cooling) in the deep-water formation region. Thus, the enhanced surface buoyancy gain (heating) in the cyclonic gyre is balanced with the enhanced surface buoyancy loss (cooling) in the deep-water formation region.

The vertical diffusion at the subsurface depths in the region with Ekman upwelling dominates over that in the rest of the ocean. The intensified basin-scale overturning circulation with enhanced surface buoyancy fluxes is reproduced for the case without wind stress where the vertical diffusivity is locally enhanced; that is, the vertical diffusivity is enhanced at the subsurface depths in the region corresponding to the cyclonic wind-driven gyre. Thus, it can be said that this intensified overturning circulation is due to the thermohaline circulation enhanced by wind forcing, not being driven directly by the wind. This thermohaline circulation can be called the wind-enhanced thermohaline circulation, which connects the deep-water formation region to the cyclonic wind-driven gyre. Its intensity becomes weaker with increasing vertical diffusivity.

In the real ocean, the wind-enhanced thermohaline circulation is expected to connect a water-mass formation region to a region with Ekman upwelling. As pointed out in Toggweiler and Samuels (1995) for NADW, the existing knowledge of the thermohaline circulation cannot account for the magnitude of the meridional overturning circulation. The wind-enhanced thermohaline circulation may complement this shortage. In fact, Hasumi and Suginohara (1999a,b) clearly demonstrate that the wind-enhanced thermohaline circulation is found in both the Atlantic and the Pacific in their World Ocean circulation model with a high accuracy tracer advection scheme, UTOPIA/QUICKEST (Leonard et al. 1993), which enables them to adopt the observed small vertical diffusion coefficient, $K_V = 0.1\ \text{cm}^2\ \text{s}^{-1}$ (Ledwell et al. 1993).

Here it is necessary to discuss the applicability of the present result to a coupled ocean–atmosphere system. It is naturally accepted that in an ocean-only model the wind-induced upwelling causes a buoyancy gain as long as the surface boundary condition for the thermohaline forcing is in the form of restoring to the observed temperature and salinity (e.g., Tsujino and Suginohara 1998). However, in the coupled system, this type of surface boundary condition is suitable only for the surface heat flux but not for the surface freshwater flux. That is, precipitation and evaporation are not directly related to the wind-induced upwelling, though the upwelling leads to changes in the thermal environments at the sea surface. To evaluate properly the effect of the wind forcing on the thermohaline circulation it is necessary to use a coupled ocean–atmosphere model.

*Acknowledgments.* We would like to thank Shigeaki Aoki, Ryo Furue, and Hiroyasu Hasumi for pleasant discussions and helpful comments. Thanks are extended to two anonymous reviewers for valuable comments. All the figures in this paper are drawn with graphic routines in GFD-Dennou Library, developed by GFD-Dennou Club.

REFERENCES

Bryan, K., 1984: Accelerating the convergence to equilibrium of ocean–climate models. *J. Phys. Oceanogr.,* **14,** 666–673.

Hasumi, H., and N. Suginohara, 1999a: Sensitivity of a global ocean circulation model to tracer advection schemes. *J. Phys. Oceanogr.,* in press.

——, and ——, 1999b: Atlantic deep circulation controlled by heating in the Southern Ocean. *Geophys. Res. Lett.,* in press.

Ishizaki, H., 1994: A simulation of the abyssal circulation in the North Pacific Ocean. Part I: Flow field and comparison with observations. *J. Phys. Oceanogr.,* **24,** 1921–1939.

Ledwell, J., A. J. Watson, and C. L. Law, 1993: Evidence for slow mixing across the pycnocline from an open-ocean tracer-release experiment. *Nature,* **364,** 701–703.

Leonard, B., M. K. MacVean, and A. P. Lock, 1993: Positivity-preserving numerical schemes for multidimensional advection. NASA Tech. Memo. 106055, ICOMP-93-05, 62 pp.

Luyten, J., J. Pedlosky, and H. Stommel, 1983: The ventilated thermocline. *J. Phys. Oceanogr.*, **13,** 292–309.
Nakata, M., and N. Suginohara, 1998: Role of deep stratification in transporting deep water from the Atlantic to the Pacific. *J. Geophys. Res.*, **103,** 1067–1086.
Obata, A., R. Furue, S. Aoki, and N. Suginohara, 1996: Modeling layered structure in deep Pacific circulation. *J. Geophys. Res.*, **101,** 3663–3674.
Samelson, R., and G. K. Vallis, 1997: Large-scale circulation with small diapycnal diffusion: The two-thermocline limit. *J. Mar. Res.*, **55,** 223–275.
Suginogara, N., and S. Aoki, 1991: Buoyancy-driven circulation as horizontal convection on $\beta$-plane. *J. Mar. Res.*, **49,** 295–320.
Toggweiler, J., and B. Samuels, 1995: Effect of Drake Passage on the global thermohaline circulation. *Deep-Sea Res.*, **42,** 477–500.
Tsujino, H., and N. Suginohara, 1998: Thermohaline effects on upper layer circulation of the North Pacific. *J. Geophys. Res.*, **103,** 18 665–18 679.